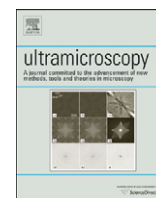




ELSEVIER

Contents lists available at ScienceDirect

Ultramicroscopy

journal homepage: www.elsevier.com/locate/ultramicHigh accuracy FIONA–AFM hybrid imaging[☆]D.N. Fronczek^a, C. Quammen^b, H. Wang^c, C. Kisker^a, R. Superfine^{b,d}, R. Taylor^b, D.A. Erie^e, I. Tessmer^{a,*}^a Rudolf Virchow Center for Experimental Biomedicine, University of Würzburg, Josef Schneider Strasse 2, 97080 Würzburg, Germany^b Computer Integrated Systems for Microscopy and Manipulation CISMM, Department of Computer Science, University of North Carolina at Chapel Hill, NC 27599-3175, USA^c Department of Pharmacology and Chemical Biology, University of Pittsburgh School of Medicine and The University of Pittsburgh Cancer Institute, Hillman Cancer Center, Pittsburgh, PA 15213, USA^d Computer Integrated Systems for Microscopy and Manipulation CISMM, Department of Physics and Astronomy, University of North Carolina at Chapel Hill, NC 27599-3255, USA^e Department of Chemistry, University of North Carolina at Chapel Hill, NC 27599-3290, USA

ARTICLE INFO

Article history:

Received 4 July 2010

Received in revised form

3 November 2010

Accepted 11 January 2011

Available online 19 January 2011

Keywords:

Atomic force microscopy (AFM)

Fluorescence imaging with one nanometer

accuracy (FIONA)

Single molecule

Multi-protein complexes

Image registration

ABSTRACT

Multi-protein complexes are ubiquitous and play essential roles in many biological mechanisms. Single molecule imaging techniques such as electron microscopy (EM) and atomic force microscopy (AFM) are powerful methods for characterizing the structural properties of multi-protein and multi-protein–DNA complexes. However, a significant limitation to these techniques is the ability to distinguish different proteins from one another. Here, we combine high resolution fluorescence microscopy and AFM (FIONA–AFM) to allow the identification of different proteins in such complexes. Using quantum dots as fiducial markers in addition to fluorescently labeled proteins, we are able to align fluorescence and AFM information to ≥ 8 nm accuracy. This accuracy is sufficient to identify individual fluorescently labeled proteins in most multi-protein complexes. We investigate the limitations of localization precision and accuracy in fluorescence and AFM images separately and their effects on the overall registration accuracy of FIONA–AFM hybrid images. This combination of the two orthogonal techniques (FIONA and AFM) opens a wide spectrum of possible applications to the study of protein interactions, because AFM can yield high resolution (5–10 nm) information about the conformational properties of multi-protein complexes and the fluorescence can indicate spatial relationships of the proteins in the complexes.

© 2011 Elsevier B.V. All rights reserved.

1. Introduction

Single molecule imaging techniques such as electron microscopy (EM) or atomic force microscopy (AFM) are well established, powerful tools for high-resolution structural characterization of essential biological molecules such as proteins and their interactions. A major limitation to these techniques, however, is the ability to distinguish different proteins. For EM, labeling of specific protein targets with biological or metal particles for protein differentiation has been previously described [1,2]. Here, we show integration of fluorescence signals into AFM data to mark specifically labeled protein molecules in the images with high accuracy

[☆] Author contributions: DAE and IT developed the concept; RS advised on technical development; IT designed the experiments; DF, CQ, and RT developed the registration and quality assessment algorithms; DF and IT performed the experiments and analyzed the data; DF carried out simulations; RT provided advice on data analysis; CK and HW provided plasmid DNA; HW performed DNA damage assessment; CK provided funding; IT wrote the manuscript; all authors edited the manuscript and provided conceptual advice.

* Corresponding author.

E-mail address: ingrid.tessmer@virchow.uni-wuerzburg.de (I. Tessmer).

(schematic shown in Fig. 1; details on setup in Supp. Information 1 and Suppl. Fig. S1).

In the last five years, there has been increasing interest in the combination of optical approaches and AFM [3–10], and integrated set-ups are available from different AFM manufacturers. Some commercial systems also provide software that allows overlay of optical and AFM images. The resulting images exploit the complementary power of fluorescence and AFM imaging, which has been elegantly demonstrated previously [6–10]. In the aligned and overlaid hybrid images, the AFM image provides the overall conformational properties of the particles in the sample and the positions of the fluorescence signals identify the fluorescently labeled molecules. However, the current methods focus on overlaying images of multiply fluorescently labeled supramolecular assemblies. Recently, Sanchez and colleagues have presented a method for combining AFM and fluorescence microscopy using multiply labeled “nano-spheres” as fiducial markers. Registration of the positions of these markers in the AFM and fluorescence images provides such aligned hybrid overlay images in which they showed good positional agreement of fluorescence and topography signals qualitatively and for multiply labeled systems. However, the small size of protein

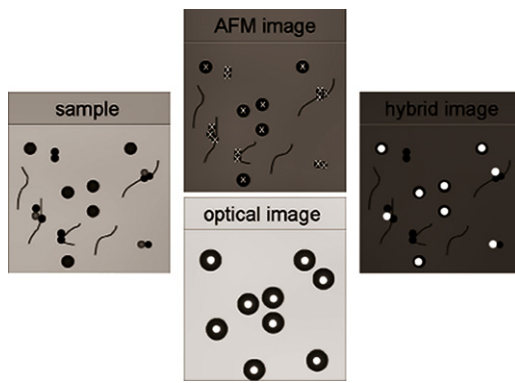


Fig. 1. Principle of FIONA-AFM: A sample of protein 1 (small black filled circles) and fluorescently labeled protein 2 (small light gray filled circles) that form heteromeric multi-protein complexes on DNA (black lines) is imaged simultaneously by AFM and by fluorescence microscopy. Quantum dots (QDs; large dark gray filled circles) are added to the sample to provide fiducial markers. In the AFM image, all particles in the sample are visible but not necessarily distinguishable. In the optical image, only the fluorescently labeled protein 2 and the QDs are resolved. Center tracking algorithms are applied to the AFM and fluorescence images, separately (white crosses in AFM image, white filled circles in optical image). Displaying the fluorescence centers as Gaussian peaks with widths reflecting localization accuracy of each fluorescence signal, provides FIONA images from the raw fluorescence data. QDs have distinct signals in both the topographical AFM and the fluorescence images. For this reason we can use the center-tracked QD peaks for alignment of the two types of images. The registration algorithm requires manual coarse selection of at least four mutual points (fiducial markers) in the two images and determines the optimal affine alignment transformation using a weighted least squares optimiser. In the resulting FIONA-AFM image, fluorescent signals (here: white filled circles) highlight the labeled protein 2 molecules and the QDs in the topographical images.

complexes (with typical dimensions of individual protein molecules between 5 and 50 nm) necessitates extremely high image registration accuracy to ensure identification of the correct, fluorescently labeled particle by its fluorescent signal in the overlay images. In this work we establish conditions and parameters for optimized and controllable image overlay accuracy to enable the identification of individual single molecules within the context of biological complexes. In our experiments, we use quantum dots, which provide single fluorophore point light sources, as fiducial markers for image registration (see also Supp. Information 2). We carried out extensive error analysis to evaluate and optimize image overlay accuracy (see Section 3). Here, we demonstrate the overlay of fluorescence and AFM images of QDs (Fig. 2) and of QD-labeled UvrA–UvrB–DNA complexes (Fig. 3) with ~ 10 nm accuracy. Notably, this order of overlay accuracy is also the optimum achieved for the overlay of separately acquired fluorescence images of the same sample area [11].

2. Methods

2.1. Biological sample preparation

2.1.1. UvrA and UvrB expression and purification, UvrB–QD conjugation

UvrA wild type and UvrB $\Delta 4$ (a UvrB mutant missing domain 4) from *Bacillus caldotenax* were expressed and purified using the IMPACTTM-CN system (New England Biolabs) followed by size exclusion chromatography (Superdex 200 26/60; GE Health Care) as described [12]. As in the precursor AFM study using QD–UvrB conjugation, the UvrB $\Delta 4$ mutant is employed because of its enhanced binding to DNA compared to the wild type protein, and QDs are conjugated to UvrB $\Delta 4$ as described at QD:protein ratio of 5:1 [13]. Briefly, UvrB $\Delta 4$ carries a hemagglutinin tag that

enables the conjugation to QDs (Quantum dot 605 goat F(ab')₂ anti-mouse IgG conjugate, Invitrogen, 1 μ M) via an antibody sandwich linker. Proteins used in this study are greater than 95% pure as judged by Coomassie Blue stained SDS-PAGE. We have previously shown functionality for the QD–protein conjugate in DNA binding [13]. The conjugation process does not significantly affect the fluorescence emission properties of the QDs in the images (data not shown).

2.1.2. UV irradiated DNA

UV irradiation induced photoproducts in DNA are target sites for UvrA–UvrB complexes. Lambda phage DNA (48,502 bp) was obtained from Sigma–Aldrich as lyophilized powder, dissolved in purified water (> 18 M Ω cm⁻¹) to a concentration of approximately 10 nM, and damaged by exposure to UV irradiation for 30 min (300 nm wavelength, 15 W; UV Transilluminator, Ultralum Inc.). The DNA was then concentrated to 70 nM using a 50 kD MWCO centrifuge filter (Microcon, Millipore). Successful introduction of UV damages in the DNA is demonstrated using agarose gel electrophoresis (0.5% agarose, 1 \times TBE buffer, 3 h at 100 V; data not shown). We confirmed the presence of a minimum of 1 lesion/4000 base pairs in the DNA, using a quantitative PCR assay as previously described [14].

2.2. Experimental sample preparation

FIONA–AFM of protein–DNA complexes requires imaging on extremely thin mica substrate (≤ 50 μ m, see text). We prepared thin mica slides by cutting approximately 1 \times 2 cm² from larger pieces of grade V muscovite mica (SPI Supplies) and splitting them into thinner slices using a scalpel. Mica thickness can be measured using a micrometer caliber. These pre-skimmed mica substrates were further freshly stripped using conventional adhesion tape immediately prior to sample deposition. Samples of non-conjugated QDs were diluted in AFM deposition buffer (25 mM HEPES pH 7.5, 25 mM Na–Acetate, 5 mM Mg–Acetate) to a concentration of approximately 100 pM (Fig. 2). UvrA–UvrB/QD–DNA complexes were incubated for 30 min at ambient temperature at concentrations of 12 nM UvrA/UvrB, 60 nM QD (5-fold excess over UvrB), 40 nM DNA in incubation buffer (50 mM Tris–HCl pH 7.5, 50 mM KCl, 10 mM MgCl₂, 1 mM ATP). Prior to incubation with UvrA–UvrB for AFM imaging, the DNA was heated to 65 $^{\circ}$ C for 10 min to melt and remove potential salt crystals from the DNA. For deposition, UvrA–UvrB/QD–DNA samples were diluted 150-fold in deposition buffer. Immediately after dilution in deposition buffer, small volumes (20 μ l) of sample solution were deposited on freshly cleaved mica, rinsed with purified deionized water, dried in a stream of nitrogen, and imaged.

2.3. Image acquisition

2.3.1. AFM

AFM imaging was carried out in air in oscillating mode using OMCL-AC240TS (Olympus) noncontact/tapping mode silicon probes with spring constants of ~ 2 N/m and resonance frequencies of ~ 70 kHz. Images were captured at scan sizes of 16 \times 16 and 8 \times 8 μ m², at a scan speed of 3 μ m/s (corresponding to scan rates of 0.07 and 0.15 Hz for 16 \times 16 and 8 \times 8 μ m² images, respectively) and at resolutions of 2048 \times 2048 or 1024 \times 1024 pixels.

2.3.2. Fluorescence

A series of fluorescence images are recorded each with an integration time of 0.5 s at non-saturating EM gain. For image registration, a sum image is produced from these individual images

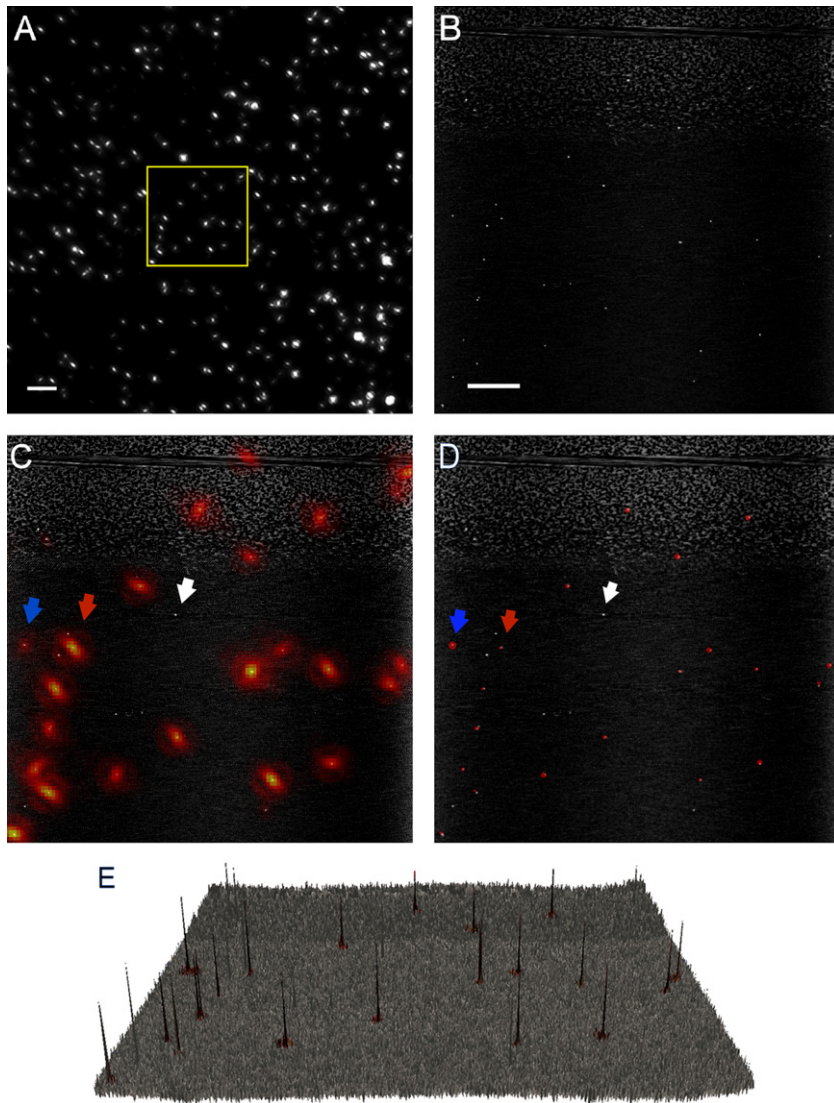


Fig. 2. FIONA-AFM image registration: QD sample imaged by (A) fluorescence microscopy and (B) AFM. Scale bars are 4 μm (A) and 1 μm (B). The fluorescence image is the sum of approximately 20 individual CCD images with integration time 0.5 s each. The region of interest (AFM scan area) is located around the center of the fluorescence image and is indicated by a yellow box. (C–E) Hybrid overlay images of the area shown in (B): (C) raw fluorescence signals with AFM topography; (D and E) FIONA signals with AFM topography. AFM signal is shown as gray-scale top view image (B–D) or 3D topography (E), fluorescence is shown overlaid in color. Due to QD blinking, a fraction of particles does not emit fluorescence during the time of detection (for example white arrow in C and D). Displaying fluorescence data not as the broad, diffraction-limited raw signals (as in A and C) but as Gaussian distributions around the fluorescence centers (localization probability distribution) as given by FIONA fits of multiple fluorescence images provides peak dimensions typically < 10 nm (D and E). These peak diameters closely match those of the particles in the AFM topography images. Because the centers of higher SNR signals can be localized with higher accuracy than those of low SNR signals, the widths of the probability distributions are inversely proportional to signal intensity (see e.g. in (C and D) blue arrow indicating low SNR and orange arrow indicating high SNR particle, with approximate SNRs of 9 and 16, respectively). Pixel resolution is 7.8 nm/pixel. QDs appear between 4 and 6.5 nm high while their nominal diameter including the softer polymer and biological coatings is approximately 20 nm, consistent with previous studies.[13] Good positional agreement of fluorescence and AFM peaks is observed in the images: we notice that all FIONA peaks (red color) are overlaid on the AFM topography peaks of the QDs. Optimal image registration accuracy of 8 nm was achieved using $n=7$ fiducial markers with $\text{SNR} > 13$.

with a total summed integration time of approximately 10 s, to minimize the effect of missing fluorescence signals in the images due to QD blinking.

2.4. Image registration and error analysis

In order to overlay fluorescence and AFM images, center positions of the fiducial markers must be located in the two types of images. In the AFM topographic image, center localization is achieved using a local maximum tracker and in the fluorescence image using a FIONA tracker which fits a 2D-Gaussian function to the fluorescence signals. For the near-spherical QDs, maximum height corresponds well with the center of the particle. The local

maximum tracker provides the position of the pixel with maximum height as particle center, so that position uncertainty for center localization is limited to approximately half the AFM pixel size. Uncertainties in the FIONA center positions of the fluorescence signals are evaluated by fitting of several (approximately 20) images of the same area and comparing the reported positions, as has been previously applied to other localization algorithms [15].

Fluorescence and AFM images are then registered with each other by manually selecting at least four mutual fiducial marker center positions to determine the affine transformation that provides optimum image overlay. This procedure is achieved by numerically minimizing positional deviation between fluorescence and topography signals of the markers using weighted least squares optimization in a landmark-based registration

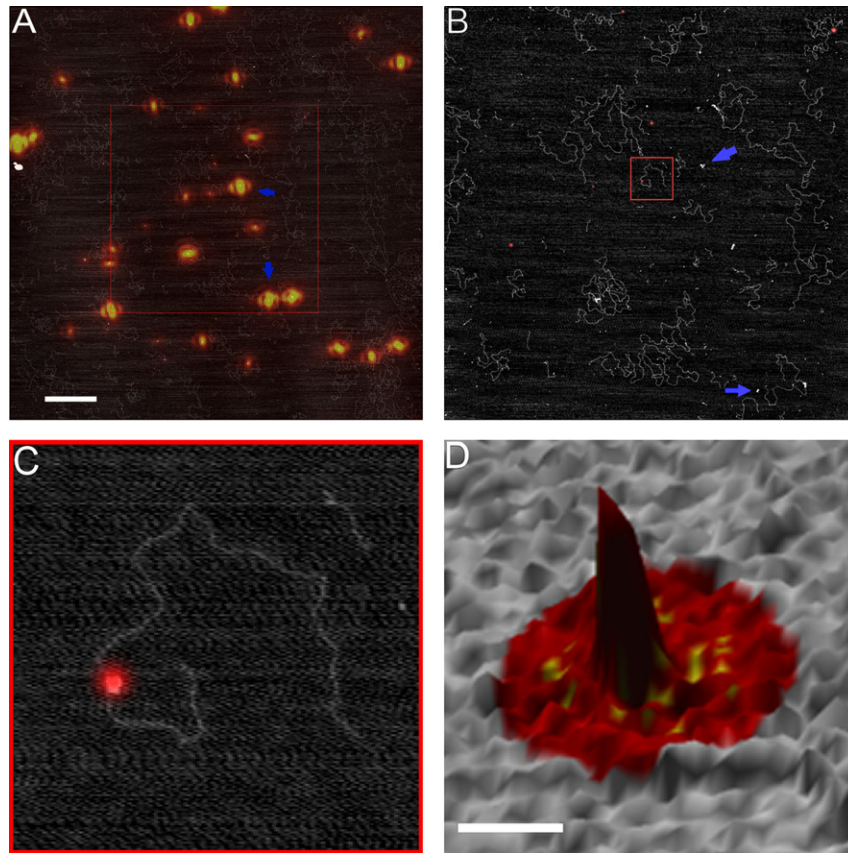


Fig. 3. FIONA-AFM of UvrA-UvrB-QD complexes with UV-damaged DNA: Registration of the raw fluorescence signals with AFM topography of the same sample area is shown in (A). Fluorescence is shown as red color (with yellow light center for easier visualization of AFM features) overlaid on AFM topography. The scale bar in (A) is $2\ \mu\text{m}$, height scale $2\ \text{nm}$, pixel resolution $7.8\ \text{nm}/\text{pixel}$. A higher resolution display of the red boxed area in (A) of $8 \times 8\ \mu\text{m}^2$ is shown in (B) with $< 4\ \text{nm}/\text{pixel}$. In (B), fluorescence signals are shown as FIONA signals in red, corresponding to area of localization probability of the fluorescence centers. The red box in (B) indicates the QD-protein-DNA complex shown in (C and D) as top view and 3D representation, respectively. The scale bar in (D) corresponds to $30\ \text{nm}$. These zoom in figures demonstrate good FIONA-AFM overlay accuracy. Clusters of and closely co-localized QDs (which can result from the formation of protein complexes containing more than one molecule of UvrB) can be seen in the image (for example blue arrows in (A and B)). Such closely localized fluorescence sources can lead to distorted signals (see (A)) and large inaccuracies in image alignment and are therefore not included in the image registration process and not resolved in the FIONA-AFM image (B). Optimal FIONA-AFM image registration accuracy of $13.6 \pm 8.3\ \text{nm}$ was achieved using 7 QD fiducial markers with SNRs between 8 and 16. Different FIONA signal widths (in (B)) reflect different accuracies of fluorescence center localization (average FIONA accuracy $8.7\ \text{nm}$). Individual fluorescence and AFM data are shown in Supplementary Fig. 4.

procedure. Each marker is weighted with the inverse of the uncertainty of the corresponding positions [16]. The registration algorithm is written in Mathematica and is currently being integrated into the commercially available NanoManipulator[®] software package. As an indicator for the quality of the registration, the registration software supplies the mean distance between topographical AFM and FIONA centers of the fiducial markers (referred to as fiducial marker registration accuracy). Application of this optimized transformation to the FIONA-fit fluorescence image generates an output image that displays the positions of all optical labels at the correct locations in the AFM image (with accuracy referred to as image registration accuracy). The registered set of images can then be overlaid using standard visualization software.

To further optimize the resulting fluorescence-AFM overlay representation, the fluorescence signals can be displayed as 2D-Gaussians around the center positions determined by the FIONA fitting algorithm. The widths of these Gaussian peaks is given by the positional accuracies as determined from FIONA fits of ten to twenty images of the same sample area (referred to as FIONA accuracy, typically $< 10\ \text{nm}$). The resulting FIONA peaks, hence, exhibit similar widths as the actual dimensions of the fiducial markers in the AFM images as well as typical enzymes,

thus providing well-matched hybrid fluorescence-topography peaks in the FIONA-AFM images.

Their unambiguous identification in fluorescence as well as in AFM images clearly qualifies QDs as an ideal system to provide proof of principle for accurate fluorescence-AFM image overlay. To evaluate image registration accuracy, we measured the mean distance of centers of QDs that are not used for registration in the two types of images. The results given for image registration accuracy were obtained using a “leave-one-out” approach, in which alternating sets of $n-1$ of a total of n QDs are selected as fiducial markers and the positional deviation between FIONA and AFM centers of the non-selected QD is measured. For Fig. 2, image overlay accuracy of $8.0 \pm 3.0\ \text{nm}$ is achieved using $n=7$ fiducial markers with $\text{SNR} > 13$. Individual inaccuracies from FIONA and AFM images are $\Delta\text{FIONA}=5.3$ and $\Delta\text{AFM}=3.9\ \text{nm}$, respectively, and the fiducial marker registration accuracy $\Delta\text{registration}_{\text{fiducials}}=3.9\ \text{nm}$. Using fiducial markers of lower SNRs results in reduced registration accuracy consistent with our simulation results (Suppl. Fig. S2): $\Delta\text{registration}_{\text{fiducials}}=5.7\ \text{nm}$, image overlay accuracy ($8.9 \pm 6.6\ \text{nm}$) for $\text{SNR} > 12$ ($n=9$); $\Delta\text{registration}_{\text{fiducials}}=8.1\ \text{nm}$, image overlay accuracy ($11.6 \pm 7.9\ \text{nm}$) using all available QDs ($n=12$) with SNRs ranges from 11 to 15. For Fig. 3, we obtain image registration accuracy of $13.6 \pm 8.3\ \text{nm}$ using $n=7$ fiducial markers with SNRs

ranging from 8 to 16, with $\Delta_{\text{FIONA}}=8.7$ nm, $\Delta_{\text{AFM}}=7.8$ nm, and $\Delta_{\text{registration}_{\text{fiducials}}}=7.7$ nm.

3. Results and discussion

3.1. FIONA–AFM of protein complexes

We add fluorescent quantum dots (QDs) to samples containing a mixture of fluorescently labeled and non-labeled molecules and image the samples separately by AFM and total internal reflection fluorescence (TIRF) microscopy. Because we can visualize and unambiguously identify the QDs in the fluorescence as well as in the AFM images [8,13], we can exploit them as fiducial markers for fluorescence–AFM image alignment. Our approach takes advantage of a relatively new technique called FIONA (fluorescence imaging with one nanometer accuracy) in which the positions of the centers of the individual fluorophores can be located to within 1.5 nm in the fluorescence images by fitting two-dimensional Gaussian curves to their emission signal point spread functions [17]. Center localization accuracy in the fluorescence images is limited by the quality of the signals, given by their shapes and signal-to-noise ratio (SNR). To obtain the QD centers in the AFM images, we apply a local-maximum algorithm to the data that determines the image pixels with the highest topography signals, which for the near-spherical (slightly elongated elliptical) shapes of the QDs coincide well with the centers of the particles. Center localization in AFM images is therefore limited by AFM pixel resolution, to approximately half the pixel size, typically on the order of a few nm (for example 2 nm for an image size of $8 \times 8 \mu\text{m}^2$ with 2048×2048 pixels). We then use the obtained center positions of the fiducial markers (QDs) in fluorescence and AFM images to align the images.

The image registration process requires at least four fiducial markers and employs weighted least squares optimization to numerically minimize the positional deviation between fluorescence and topography centers of these markers. This least-squares fit reduces the effect of zero-mean errors in the individual images, thus potentially providing registration that is better than the localization accuracy for individual points in AFM or FIONA. By displaying the registered fluorescence signals as probability distributions of the fluorophore center locations obtained from the FIONA fit to the data (see Section 2.4), we produce FIONA–AFM images from the raw fluorescence–AFM overlay images. In these FIONA–AFM images, fluorescence signal dimensions are significantly reduced (typically >20-fold, compare e.g. Fig. 2A and B) compared to the raw fluorescence signals (with diffraction limited diameters of a few hundred nm in the visible optical spectrum), closely matching particle dimensions in the AFM images.

FIONA–AFM imaging opens the door to the elucidation of protein complex stoichiometries and relative orientations of the proteins to one another and to the DNA at the level of the individual molecules to enhance our understanding of the underlying mechanistic processes (see also Supporting Information 5). Since protein complexes are extremely small, AFM imaging of these structures requires extremely smooth and flat substrate surfaces for sample deposition. AFM imaging of larger biological structures such as cells or cytoskeletal fibers can be obtained on glass which is also a suitable substrate for fluorescence imaging. In contrast, for imaging of the much smaller proteins and protein complexes the most commonly employed AFM substrate is muscovite mica (with an average roughness of 0.05 nm versus approximately 0.5 nm for glass). However, for fluorescence microscopy, mica possesses two unfavorable properties: light absorbance and birefringence [18], causing decreased SNR and distortions of the fluorescence signals, respectively, which lead

to reduced center location and ultimately image registration accuracies [19]. We analyzed the effects of signal distortion and SNR on registration accuracy in simulation studies (Suppl. Information 3). Our results suggest that SNRs of approximately 13 or higher are required for sufficiently high positional accuracies (≤ 10 nm, Suppl. Fig. S2). We also observe fast deterioration in accuracy with decreasing SNR for signals that are majorly distorted due to birefringence, but not for the perfectly Gaussian shaped or elliptically shaped signals (Suppl. Fig. S3). For optimum quality fluorescence signals (enabling maximum image localization and registration accuracy), we optimized substrate preparation: we prepare extremely thin mica substrates ($\leq 50 \mu\text{m}$; see Section 2.2), which in contrast to the thicker mica plates typically used in AFM experiments neither give rise to any significant amounts of laser light absorption nor introduce signal distortion (see Suppl. Fig. S3).

3.2. Image registration accuracy

The accuracy of the alignment of fluorescence and AFM images depends on the localization accuracies of particle centers in the individual fluorescence and AFM images (see above), the number of fiducial markers and their SNRs. To experimentally examine the accuracy of alignment achieved, we take advantage of the unambiguous QD signals in both types of images to directly measure the deviations between fluorescence and AFM positions. We use a leave-one-out approach to evaluate image registration quality (described in Section 2.4). For the overlay shown in Fig. 2, optimal image registration accuracy of 8.0 ± 3.0 nm was obtained using 7 QDs with SNRs > 13 (with FIONA and AFM accuracies of 5.3 and 3.9 nm, respectively). Including additional QDs (total of 12 QDs) with lower SNRs reduces the accuracy of the alignment, consistent with our simulations (Section 2.4 and Suppl. Fig. S2). This alignment accuracy is in the order of the size of enzymes and should be applicable to the characterization of the conformations of multi-protein and multi-protein–DNA complexes. Furthermore, as indicated by our simulations (Suppl. Fig. S2) the quality of the alignment could be improved to ~ 4 nm (for this AFM pixel resolution) by improving the SNR of the fluorescence signal (e.g. by imaging in solution instead of air). Current theoretical and practical limitations of FIONA–AFM are summarized and discussed in more detail in the supplementary section (Suppl. Information 4).

3.3. Application to protein–DNA complexes

To demonstrate the potential of FIONA–AFM in the context of a biological system, we use QD-labeling of protein molecules so that in addition to serving as fiducial markers, QDs here also indicate the positions of the labeled protein molecules. In the future, we will employ organic fluorophores rather than QDs for protein labeling, as shown in Fig. 1. But here we are again taking advantage of their distinct topographical as well as fluorescent signals to directly measure image overlay accuracy. In our experiments, we incubate UvrB conjugated to QDs, together with UvrA and damaged DNA. The UvrA–UvrB multi-protein–DNA complex is responsible for initiation of nucleotide excision repair (NER) in bacteria. NER is a major DNA repair pathway that is highly conserved in all organisms and is responsible for the removal of a wide spectrum of DNA lesions, including UV irradiation induced damages [20]. We previously demonstrated conjugation of UvrB to QDs at one-to-one stoichiometry and that QD-labeling allows unambiguous identification of UvrB in the two different stages of DNA damage recognition of NER, namely the UvrA–UvrB–DNA and UvrB–DNA complexes, in AFM images [13]. Fig. 3 shows

FIONA–AFM overlay images of UvrA and UvrB–QD conjugate deposited in the presence of lambda phage DNA containing multiple UV-induced thymine–dimers (Section 2.1). Non-conjugated QDs remain free (non-DNA bound) on the surface, consistent with previous studies [13]. In addition, co-localization or clustering of QDs, which may result from formation of UvrAB complexes containing more than one UvrB, are seen in the images (Fig. 3). These closely co-localized QDs cannot be accurately located using FIONA, and are therefore not included in the FIONA–AFM image (Fig. 3B). We are currently developing an algorithm to resolve multiple fluorescence signals that are co-localized within the diffraction limit (Supp. Information 5). Optimal alignment of FIONA and AFM images shown in Fig. 3 was obtained using 7 fiducial markers (QDs) with SNRs between 8 and 16. The image registration accuracy is 13.6 ± 8.3 nm, FIONA and AFM localization accuracies are 8.7 and 7.8 nm, respectively (see Section 2.4). The zoomed-in image (Fig. 3C and D) demonstrates accurate co-localization of the FIONA signal on a QD–UvrB–DNA complex.

4. Conclusions

In summary, FIONA–AFM provides hybrid images containing fluorescence and topographic information with high (~ 10 nm) localization accuracy, which can be still further enhanced by increasing fluorescence SNR and/or AFM pixel resolution. QD-conjugation to proteins enables us to evaluate fluorescence–AFM image registration accuracy. We are currently optimizing FIONA–AFM using proteins labeled with organic fluorophores (as has been previously described for single molecule applications with high SNR ratios > 30 on glass in solution) [17] and non-conjugated QDs added as fiducial markers (as shown in the schematic in Fig. 1).

Acknowledgements

This work was supported by grants from the Deutsche Forschungsgemeinschaft (DFG; Forschungszentrum FZ82) to CK and IT. IT and DF would like to thank Bennett Van Houten for

fruitful discussions on DNA repair and Gudrun Michels for assistance with protein preparation.

Appendix A. Supplemental Information

Supplementary data associated with this article can be found in the online version at doi:10.1016/j.ultramic.2011.01.020.

References

- [1] U. Ziese, C. Kubel, A. Verkleij, A.J. Koster, J. Struct. Biol. 138 (2002) 58–62.
- [2] P.D. Chastain 2nd, J.L. Bowers, D.G. Lee, S.P. Bell, J.D. Griffith, J. Biol. Chem. 279 (2004) 36354–36362.
- [3] W. Liu, L.M. Jawerth, E.A. Sparks, M.R. Falvo, R.R. Hantgan, R. Superfine, S.T. Lord, M. Guthold, Science 313 (2006) 634.
- [4] F. Lin, K.E. Elliott, W. Parker, N. Chakraborty, C.S. Theo, S.T. Smith, G.D. Elliott, P.J. Moyer, Rev. Sci. Instrum. 80 (2009) 055110.
- [5] H. Gump, S.W. Stahl, M. Strackharn, E.M. Puchner, H.E. Gaub, Rev. Sci. Instrum. 80 (2009) 063704.
- [6] J. Oreopoulos, C.M. Yip, J. Struct. Biol. 168 (2009) 21–36.
- [7] H. Sanchez, R. Kanaar, C. Wyman, Ultramicroscopy 110 (2010) 844–851.
- [8] Y. Ebenstein, N. Gassman, S. Kim, S. Weiss, J. Mol. Recognit. 22 (2009) 397–402.
- [9] M.S. Kellermayer, A. Karsai, A. Kengyel, A. Nagy, P. Bianco, T. Huber, A. Kulcsar, C. Niedetzky, R. Proksch, L. Grama, Biophys. J. 91 (2006) 2665–2677.
- [10] K.-I. Shinohara, T. Suzuki, T. Kitami, S. Yamaguchi, J. Polym., Sci. Pol. Chem. 44 (2006) 801–809.
- [11] L.S. Churchman, Z. Okten, R.S. Rock, J.F. Dawson, J.A. Spudich, Proc. Natl. Acad. Sci. USA 102 (2005) 1419–1423.
- [12] K. Theis, P.J. Chen, M. Skorvaga, B. Van Houten, C. Kisker, Embo. J. 18 (1999) 6899–6907.
- [13] H. Wang, I. Tessmer, D.L. Croteau, D.A. Erie, B. Van Houten, Nano Lett. 8 (2008) 1631–1637.
- [14] J.H. Santos, J.N. Meyer, B.S. Mandavilli, B. Van Houten, Methods Mol. Biol. 314 (2006) 183–199.
- [15] M.J. Rust, M. Bates, X. Zhuang, Nat. Methods 3 (2006) 793–795.
- [16] P.R. Bevington, D.K. Robinson, Data Reduction and Error Analysis for the Physical Sciences, 3rd ed., McGraw-Hill, Boston, 2003 xi, 320.
- [17] A. Yildiz, J.N. Forkey, S.A. McKinney, T. Ha, Y.E. Goldman, P.R. Selvin, Science 300 (2003) 2061–2065.
- [18] El-Bahrawi, Opt. Laser Technol. 30 (1998) 411–415.
- [19] M.K. Cheezum, W.F. Walker, W.H. Guilford, Biophys. J. 81 (2001) 2378–2388.
- [20] B. Van Houten, D.L. Croteau, M.J. DellaVecchia, H. Wang, C. Kisker, Mutat. Res. 577 (2005) 92–117.